Electrochimica Acta 54 (2009) 3851–3856

Contents lists available at ScienceDirect

Electrochimica Acta

journal homepage: www.elsevier.com/locate/electacta

Improvement of electrochemical and thermal properties of $Li[Ni_{0.8}Co_{0.1}Mn_{0.1}]O_2$ positive electrode materials by multiple metal (Al, Mg) substitution

S.-W. Woo [a], S.-T. Myung [b,**], H. Bang [a], D.-W. Kim [a], Y.-K. Sun [a,*]

[a] Department of Chemical Engineering, Center for Information and Communication Materials, Hanyang University, Seoul 133-791, South Korea
[b] Department of Chemical Engineering, Iwate University,4-3-5 Ueda, Morioka, Iwate 020-8551, Japan

ARTICLE INFO

Article history:
Received 4 December 2008
Received in revised form 14 January 2009
Accepted 18 January 2009
Available online 24 January 2009

Keywords:
$Li[Ni_{0.8}Co_{0.1}Mn_{0.1}]O_2$
Al
Mg
Substitution
Positive electrode
Lithium
Batteries

ABSTRACT

Al and/or Mg-substituted $Li[Ni_{0.8}Co_{0.1}Mn_{0.1-x-y}Al_xMg_y]O_2$ were prepared by a co-precipitation method and characterized by X-ray diffraction with Rietveld refinement, thermogravimetric analysis, differential scanning calorimetry (DSC), and electrochemical measurements. The Rietveld refinement results show that cation mixing of Al and/or Mg-substituted $Li[Ni_{0.8}Co_{0.1}Mn_{0.1-x-y}Al_xMg_y]O_2$ was reduced with increased doping amounts of Al and Mg. The Al and/or Mg substitution in $Li[Ni_{0.8}Co_{0.1}Mn_{0.1}]O_2$ also resulted in improved electrochemical cycling behavior, structural stability, and thermal stability compared to pristine $Li[Ni_{0.8}Co_{0.1}Mn_{0.1}]O_2$. The improvements of electrochemical and thermal properties resulted from the stabilized host structure by Al and/or Mg incorporation into $Li[Ni_{0.8}Co_{0.1}Mn_{0.1}]O_2$.

1. Introduction

Layered $LiNiO_2$ and its derivatives have been intensively studied to produce improved electrochemical performance of $LiNiO_2$ by a partial substitution of Ni with other metals [1–6]. Among the potential substituted materials, Co-substitution for Ni has been reported to reduce cation mixing (some Ni^{2+} ions of Ni layer move to Li layer) and enhance its structural stability due to their complete formation of a solid solution [7–12]. It has also been reported that a small amount of Al or Mg substitution for Ni in $LiNiO_2$ improved electrochemical properties such as cycling performance and thermal stability [13–18]. Ohzuku et al. reported that partial Al substitution for nickel effectively stabilizes the structure of $Li[Ni_{1-x}Al_x]O_2$ by suppressing phase transitions observed for the $LiNiO_2$ system and therefore, results in improved thermal stability [14]. Pouillerie et al. proposed that the substitution of Mg^{2+} ions, which are of a similar size to Li^+, in the lithium layer prevents local collapses of the structure during cycling, resulting in enhanced electrochemical performance in the $LiNi_{1-y}Mg_yO_2$ system [16]. Cho also studied the Mg substitution effect in the $LiNi_{0.74}Co_{0.26-x}Mg_xO_2$ system and reported that the improvement of electrochemical properties derived from the reduced cation mixing [18]. Thermal stability was also enhanced because of the structural stability accomplished by Mg substitution. The substitution of Ni by a small amount of other cations such as Ga, Nb, Ca, and Ti has been found to improve cycling stability and/or thermal stability due to suppression of the phase transitions observed for the $LiNiO_2$ system although their initial discharge capacities were reduced [19–22]. The most widely used Ni-rich material in the $Li[Ni_{1-x}M_x]O_2$ system is Co and Al co-substituted $Li[Ni_{0.8}Co_{0.15}Al_{0.05}]O_2$ due to its good thermal stability and cyclability [23–29]. An alternative material is Co and Mn co-substituted $Li[Ni_{0.8}Co_{0.1}Mn_{0.1}]O_2$ which delivers a high discharge capacity of 200 mAh g^{-1}, compared with $LiCoO_2$ (150–160 mAh g^{-1}), when cycled between 2.8 and 4.3 V [30]. However, capacity fading was inevitable during cycling. From the above studies, it is expected that a partial substitution of Al and/or Mg would have positive effect to improve battery performances. In this study, we report effects of Al and Mg co-substitution for $Li[Ni_{0.8}Co_{0.1}Mn_{0.1-x-y}Al_xMg_y]O_2$ ($x, y = 0.0–0.02$) on structure, electrochemical property, and thermal stability.

2. Experimental

To improve homogeneity of final product, $Li[Ni_{0.8}Co_{0.1}Mn_{0.1-x-y}Al_xMg_y]O_2$ (x, $y = 0.0–0.02$) samples were prepared via co-precipitation [30–32]. An aqueous solution of $NiSO_4{\cdot}6H_2O$, $CoSO_4{\cdot}7H_2O$, $MnSO_4{\cdot}5H_2O$, $MgSO_4$, and $Al(NO_3)_3{\cdot}6H_2O$ was pumped into a continuously stirred tank reactor (CSTR, capacity 4 L) under a N_2 atmosphere. At the same time, a NaOH solution (*aq.*) and a desired amount of NH_4OH solution (*aq.*) as a chelating

* Corresponding author. Tel.: +82 2 2220 0524; fax: +82 2 2282 7329.
** Co-corresponding author. Tel.: +81 19 621 6345; fax: +81 19 621 6345.
E-mail addresses: smyung@iwate-u.ac.jp (S.-T. Myung), yksun@hanyang.ac.kr (Y.-K. Sun).

0013-4686/$ – see front matter © 2009 Elsevier Ltd. All rights reserved.
doi:10.1016/j.electacta.2009.01.048

agent were also separately fed into the reactor. The spherical $[Ni_{0.8}Co_{0.1}Mn_{0.1-x-y}Al_xMg_y](OH)_2$ particles were filtered, washed, and dried in air at 120°C to remove adsorbed water. Finally, a mixture of the dehydrate $[Ni_{0.8}Co_{0.1}Mn_{0.1-x-y}Al_xMg_y](OH)_2$ and $LiOH{\cdot}H_2O$ was preheated to 480 °C for 5 h and then heated at 750 °C for 20 h under flowing oxygen [5]. An excess of lithium was used to compensate for lithium loss during the calcination.

Powder X-ray diffraction (XRD, Rigaku, Rint-2000) using Cu Kα radiation was used to identify the crystalline phase of the prepared powders at each stage. XRD data were obtained at 2θ = 10–110°, with a step size of 0.03°. The collected XRD intensity data were analyzed by the Rietveld refinement program [33]. The chemical compositions of the resulting powders were analyzed by atomic absorption spectroscopy (AAS, Vario 6, Analytic Jena AG, Jena, Germany).

Charge–discharge tests were performed with a coin type cell (R2032) at a current density of 40 mA g^{-1} (0.2 C-rate, 0.52 mA cm^{-2}) at 25 °C. The cell consisted of the positive and the lithium metal negative electrodes separated by a porous polypropylene film. The positive electrode was prepared by blending $Li[Ni_{0.8}Co_{0.1}Mn_{0.1-x-y}Al_xMg_y]O_2$, Super S carbon black, and polyvinylidene fluoride (80:10:10) in *N*-methyl-2-pyrrolidone. The slurry was then cast on aluminum foil and dried at 110 °C overnight under vacuum. The electrode area was 1.54 cm^2 with thickness of 60 μm. Load amount of the active material was about 20 mg in average. The electrolyte solution was 1 M $LiPF_6$ in a mixture of ethylene carbonate (EC) and diethyl carbonate (DEC) at a 1:1 volume ratio (Cheil Industries Inc., Korea).

Chemical extraction of lithium from the synthesized materials was carried out using NO_2BF_4 (twofold excess versus active material) in acetonitrile for several days under Ar atmosphere in a glove box. The reacted product was washed several times with acetonitrile to remove $LiBF_4$ and dried under Ar. The residual lithium amount in the chemically delithiated active material was determined by AAS. They were investigated by thermogravimetric alanysis (TG, DTG-60, SHIMADZU Industries) at a heating/cooling rate of 1 °C min^{-1}.

Differential scanning calorimetry (DSC) experiments were conducted on the chemically delithiated powders using a 200 PC (NETZSCH, Germany) instrument. Typically, 3 mg of $Li_{1-\delta}[Ni_{0.8}Co_{0.1}Mn_{0.1-x-y}Al_xMg_y]O_2$ powder and 3 μl of electrolyte were hermetically sealed inside stainless steel high pressure capsules to prevent leakage of the pressurized solvents. The DSC curves were recorded between room temperature and 350 °C at a scan rate of 5 °C min^{-1}. An empty stainless steel capsule was used as a reference pan. The weight of each sample was measured before and after the experiment. The weight was constant in all cases, indicating that there were no leaks during the experiments.

3. Results and discussion

$Li[Ni_{0.8}Co_{0.1}Mn_{0.1-x-y}Al_xMg_y]O_2$ powders were synthesized with *x* and *y* both in the range of 0.0–0.02. The chemical formulas of the powders are listed in Table 1. As can be seen in Table 1, the actual compositions were very close to the designed compositions. The XRD patterns of the $Li[Ni_{0.8}Co_{0.1}Mn_{0.1-x-y}Al_xMg_y]O_2$ powders

Table 1
Designated and observed chemical formulas of the $Li[Ni_{0.8}Co_{0.1}Mn_{0.1-x-y}Al_xMg_y]O_2$ samples measured by atomic absorption spectroscopy.

Designated chemical formula	Analyzed chemical formula
$Li[Ni_{0.8}Co_{0.1}Mn_{0.1}]O_2$	$Li[Ni_{0.795}Co_{0.103}Mn_{0.102}]O_2$
$Li[Ni_{0.8}Co_{0.1}Mn_{0.09}Al_{0.01}]O_2$	$Li[Ni_{0.795}Co_{0.103}Mn_{0.092}Al_{0.010}]O_2$
$Li[Ni_{0.8}Co_{0.1}Mn_{0.08}Al_{0.02}]O_2$	$Li[Ni_{0.792}Co_{0.101}Mn_{0.083}Al_{0.024}]O_2$
$Li[Ni_{0.8}Co_{0.1}Mn_{0.09}Mg_{0.01}]O_2$	$Li[Ni_{0.792}Co_{0.103}Mn_{0.092}Mg_{0.013}]O_2$
$Li[Ni_{0.8}Co_{0.1}Mn_{0.08}Mg_{0.02}]O_2$	$Li[Ni_{0.793}Co_{0.102}Mn_{0.084}Mg_{0.021}]O_2$
$Li[Ni_{0.8}Co_{0.1}Mn_{0.8}Al_{0.01}Mg_{0.01}]O_2$	$Li[Ni_{0.792}Co_{0.103}Mn_{0.084}Al_{0.010}Mg_{0.011}]O_2$

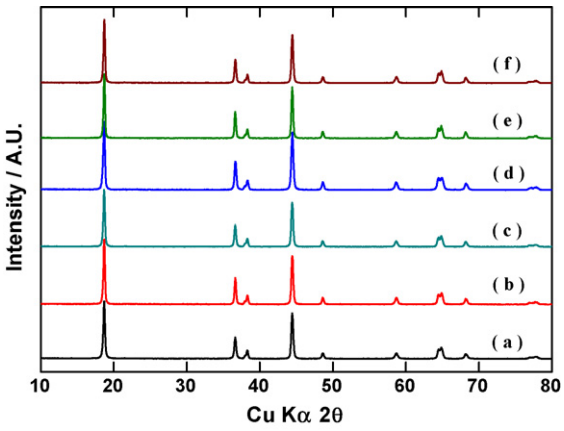

Fig. 1. XRD patterns of (a) $Li[Ni_{0.8}Co_{0.1}Mn_{0.1}]O_2$, (b) $Li[Ni_{0.8}Co_{0.1}Mn_{0.08}Al_{0.01}Mg_{0.01}]O_2$, (c) $Li[Ni_{0.8}Co_{0.1}Mn_{0.09}Al_{0.01}]O_2$, (d) $Li[Ni_{0.8}Co_{0.1}Mn_{0.08}Al_{0.02}]O_2$, (e) $Li[Ni_{0.8}Co_{0.1}Mn_{0.09}Mg_{0.01}]O_2$, and (f) $Li[Ni_{0.8}Co_{0.1}Mn_{0.08}Mg_{0.02}]O_2$.

(*x* = 0.0–0.02 and *y* = 0.0–0.02) are shown in Fig. 1. It was confirmed that all the powders have a rhombohedral α-$NaFeO_2$ structure with a space group of $R\bar{3}m$. The splits of the peaks into (0 0 6)/(0 1 2) and (0 1 8)/(1 1 0) doublets for all samples indicate the formation of a well-ordered layer structure.

Rietveld refinements based on the chemical composition obtained from AAS by assuming the space group of $R\bar{3}m$ were carried out for all the products to understand how the structures were stabilized by the replacement effects of Al and/or Mg elements,. The resultant refinement patterns and parameters are shown in Figs. 2 and 3, and Tables 2 and 3, respectively. The refinements resulted in good agreement between the observed and calculated patterns in Fig. 2(a)–(c), which indicates that Al^{3+} was well occupied in the transition metal layer, as expected. For Mg-doped $LiNi_{0.8}Co_{0.1}Mn_{0.1-y}Mg_yO_2$, we performed the refinements assuming a few different scenarios: full and partial occupation of Mg in the Li and/or Ni layers. Full occupation of Mg (*g* = 0.02) in the Li layer gave a good fit between observed and calculated patterns with the highest reliability factor, as seen in Table 2. This is natural because the ionic radius of Mg^{2+} (0.72 Å) [34] is very close to that of Li^+ (0.76 Å), so that occupation of Mg in the Li layer is highly possible.

In fact, the calculated lattice parameters of $LiNi_{0.8}Co_{0.1}Mn_{0.1}O_2$ are *a* = 2.871(1) Å and *c* = 14.190(7) Å, as seen in Fig. 3. α-$LiAlO_2$ has a smaller *a*-axis (*a* = 2.800 Å) and a larger *c*-axis (*c* = 14.220 Å) [14,35,36]. The linear decrease in the *a*-axis and increase in the *c*-axis indicate that a solid solution with α-$LiAlO_2$ was formed. Furthermore, cation mixing could be reduced by Al replacements with the transition metal element. For Mg substitution for Mn sites in $LiNi_{0.8}Co_{0.1}Mn_{0.1}O_2$, the resulting cation mixing was also slightly decreased compared to that of the pristine sample in Fig. 3. Since the Mg^{2+} was preferentially located in the Li layer, thus the total amount of Ni^{2+} occupied in the Li layer is reduced, $[Li_{0.968}Ni^{II}_{0.011}Mg^{II}_{0.021}][Ni^{III}_{0.989}Ni^{II}_{0.011}]O_2$. Compared with the $LiNi_{0.8}Co_{0.1}Mn_{0.1}O_2$ ($[Li_{0.959}Ni^{II}_{0.041}][Ni^{III}_{0.959}Ni^{II}_{0.041}]O_2$), the occupation of Ni^{2+} located in the Li site was slightly lowered by the Mg doping. The ionic radius of Ni^{2+} (0.69 Å [34]) is a little greater relative to Ni^{3+} (0.56 Å [34]). Thus, less presence of Ni^{2+} in the structure for the Mg doped powders may show slightly reduced lattice parameters, as shown in Fig. 3. The similar results were reported by Pouillerie et al. [37]. Those changes affected bonding distance of Li–O and M–O in Table 3. A shorter distance between the metal and oxygen for the Al-doped $LiNi_{0.8}Co_{0.1}Mn_{0.1}O_2$ was observed (Table 3). Due to lack of information about bonding energy it is hard to compare directly, but according to the Gibbs free energies of formation at 298 K [38] it is assumed that the order of the metal–oxygen bonding

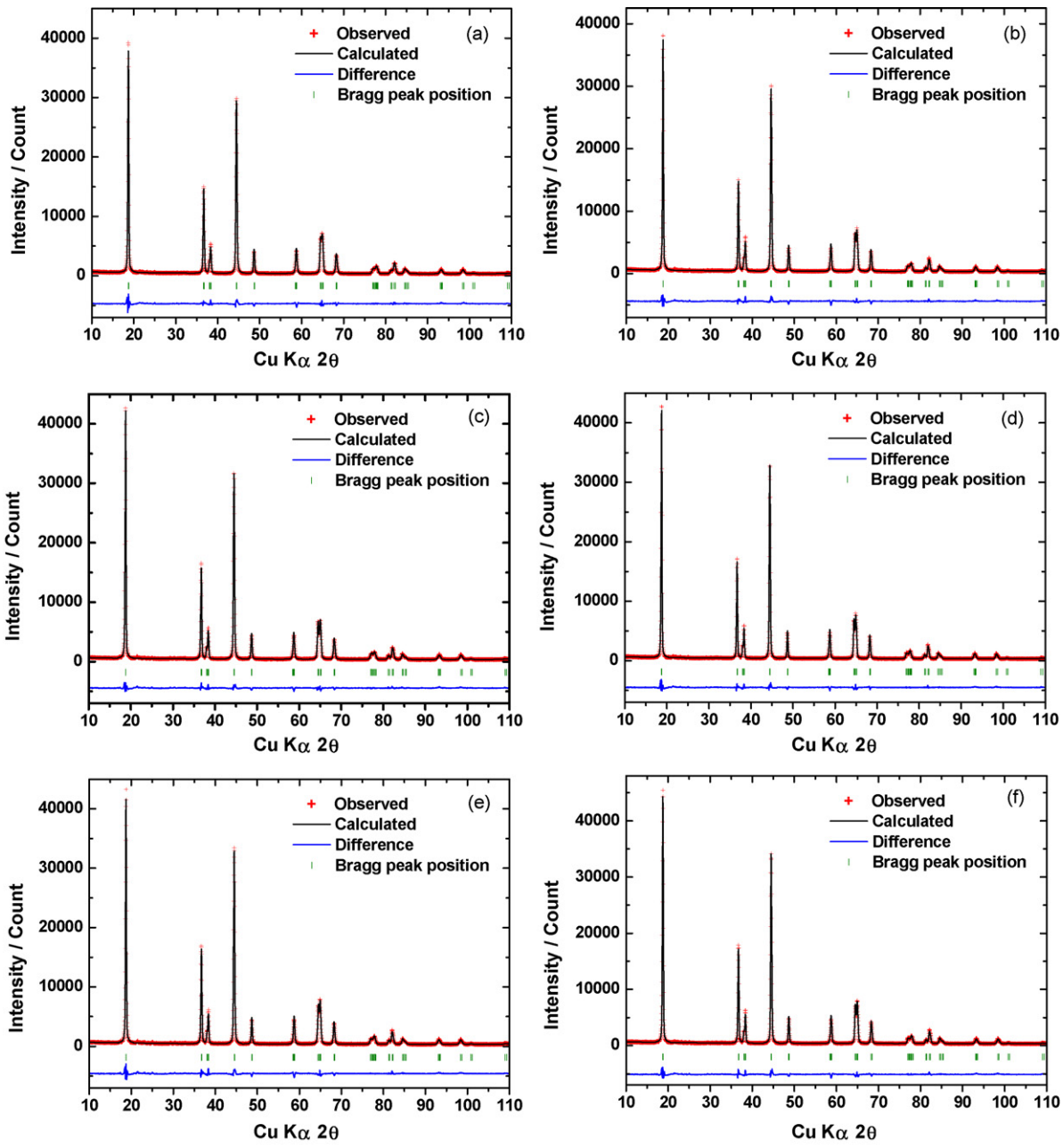

Fig. 2. Rietveld refinement patterns of the XRD data for $LiNi_{0.8}Co_{0.1}Mn_{0.1-x-y}Al_xMg_yO_2$: (a) $x = y = 0$, (b) $x = 0.01$, $y = 0$, (c) $x = 0.02$, $y = 0$, (d) $x = 0$, $y = 0.01$, (e) $x = 0$, $y = 0.02$, and (f) $x = 0.01$, $y = 0.01$.

strength is Al^{III}–O > Mn^{III}–O > Mg^{II}–O > Ni^{III}–O. It can be interpreted that the stronger bonding induced by incorporation of Al and/or Mg in the host structure would give improved structural stability.

Fig. 4 shows initial charge–discharge curves of $Li/Li[Ni_{0.8}Co_{0.1}Mn_{0.1-x-y}Al_xMg_y]O_2$ ($x = 0.0$–0.02, $y = 0.0$–0.02) cells when applying a constant current density of 40 mA g^{-1} (0.2 C-rate) between 3.0 and 4.3 V. The discharge capacity slightly decreased with the increase of Al and Mg content with 201.1 mAh g^{-1} for x and $y = 0$ (pristine), 194.3 mAh g^{-1} for $x = 0.01$ ($y = 0$), 191.7 mAh g^{-1} for $x = 0.02$ ($y = 0$), 199.6 mAh g^{-1} for $y = 0.01$ ($x = 0$), 195.8 mAh g^{-1} for $y = 0.02$ ($x = 0$), and 197.7 mAh g^{-1} for x and $y = 0.01$. The decrease in discharge capacities of the Al and Mg-doped electrodes ($Li[Ni_{0.8}Co_{0.1}Mn_{0.1-x-y}Al_xMg_y]O_2$) may be due to the decrease in concentration of the active M^{3+} (M = Ni, Co, and Mn) ions as the inactive Al and Mg content increases [39].

Fig. 5 shows the variation of discharge capacities vs. cycle number of $Li/Li[Ni_{0.8}Co_{0.1}Mn_{0.1-x-y}Al_xMg_y]O_2$ ($x = 0.0$-0.02, $y = 0.0$-0.02) cells cycled at a C-rate of 0.5 (100 mA g^{-1}) between 3.0 and 4.3 V. Although the $Li[Ni_{0.8}Co_{0.1}Mn_{0.1}]O_2$ electrode delivered the highest initial discharge capacity of 195 mAh g^{-1} at the 0.5 C-rate, it showed gradual capacity fading during cycling and exhibited a 83.5% capacity retention after 70 cycles. For the Al-substituted $Li[Ni_{0.8}Co_{0.1}Mn_{0.1-x}Al_x]O_2$ ($x = 0.01$ and 0.02) electrodes, the capacity retention was 91% while these electrodes delivered a slightly lower initial capacity of 184–185 mAh g^{-1}. The improved cycling performance of Al-substituted electrodes is attributed to the stabilization of host structure confirmed by Rietveld refinement. Ohzuku et al. [14] and Pouillerie et al. [16] performed structural characterization using XRD and they reported that Al substitution for Ni suppresses all the phase transitions observed upon cycling.

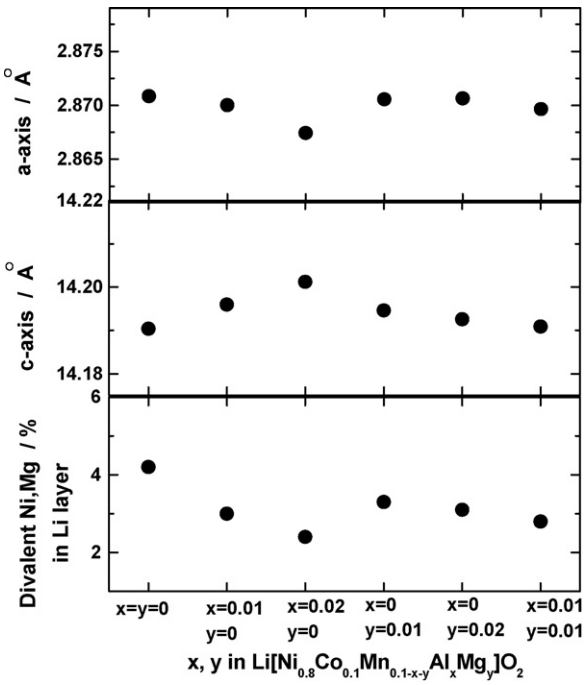

Fig. 3. Variation of the structural parameters obtained from the Rietveld refinements of the XRD data in Fig. 2.

Meanwhile, the Mg-substituted electrodes $Li[Ni_{0.8}Co_{0.1}Mn_{0.1-y}Mg_y]O_2$ ($y = 0.01$ and 0.02) had larger initial capacities of 187–190 mAh g^{-1} and showed an enhanced capacity retention of 93.3% for $y = 0.02$. This enhanced discharge capacity and capacity retention is due to the reduced cation mixing of Ni ions and suppression of structural collapse of the inter-slab space between the NiO_2 layers due to the presence of Mg ions in the lithium site (3b) by Mg substitution [37], as confirmed by the Rietveld refinement results shown in Table 2. They suggested that a small amount of Mg substitution for nickel in $LiNiO_2$ leads to an improvement of the cycling properties since the Mg^{2+} ions migrate from the 3a site (transition metal) to the 3b site (lithium site), which decrease the lattice parameters and crystallite volume variations during cycling [16,37]. The $Li[Ni_{0.8}Co_{0.1}Mn_{0.08}Al_{0.01}Mg_{0.01}]O_2$ electrode showed a capacity retention of 92% and an initial capacity of 191 mAh g^{-1}. The higher capacity is ascribed to both the reduced cation mixing and improved structural stability by Mg and Al substitution.

Table 2
Structural parameters obtained from Rietveld refinement of the XRD data of $Li[Ni_{0.8}Co_{0.1}Mn_{0.08}Al_{0.02}]O_2$ and $Li[Ni_{0.8}Co_{0.1}Mn_{0.08}Mg_{0.02}]O_2$.

Formula (experimental)					$Li[Ni_{0.792}Co_{0.101}Mn_{0.083}Al_{0.024}]O_2$	
Crystal system					Rhombohedral	
Space group					$R\bar{3}m$	
Atom	Site	x	y	z	g	B (Å^2)
Li1	3b	0	0	1/2	0.976(1)	0.63(4)
Ni2	3b	0	0	1/2	0.024(1)	0.63(4)
Ni1	3a	0	0	0	0.792	1.03(8)
Co1	3a	0	0	0	0.101	1.03(8)
Mn1	3a	0	0	0	0.083	1.03(8)
Al1	3a	0	0	0	0.024	1.03(8)
O	6c	0	0	0.259(11)	1	0.8
R_{wp} (%)		8.03				
Formula (experimental)					$Li[Ni_{0.793}Co_{0.102}Mn_{0.084}Mg_{0.021}]O_2$	
Crystal system					Rhombohedral	
Space group					$R\bar{3}m$	
Atom	Site	x	y	z	g	B (Å^2)
Li1	3b	0	0	1/2	0.968(1)	0.78(3)
Ni2	3b	0	0	1/2	0.011(1)	0.78(3)
Mg1	3b	0	0	1/2	0.021(1)	0.78(3)
Ni1	3a	0	0	0	0.810	0.91(9)
Co1	3a	0	0	0	0.104	0.91(9)
Mn1	3a	0	0	0	0.086	0.91(9)
O1	6c	0	0	0.259(12)	1	0.8
R_{wp} (%)		9.22				

(n(Li1) + n(Ni2) = 1, n(Ni1) + n(Co1) + n(Mn1) + n(Al1) = 1).

Table 3
Metal–oxygen distances of $Li[Ni_{0.8}Co_{0.1}Mn_{0.1-x-y}Al_xMg_y]O_2$ ($x = 0.0$–0.02, $y = 0.0$–0.02). The distances were calculated from Rietveld refinements of XRD data.

$Li[Ni_{0.8}Co_{0.1}Mn_{0.1-x-y}Al_xMg_y]O_2$	Li–O (Å)	M–O (Å)	R_{wp} (%)	R_p (%)
$x = 0$, $y = 0$	2.1095(13)	1.9676(11)	8.73	7.64
$x = 0.01$, $y = 0$	2.1108(12)	1.9662(12)	8.81	7.49
$x = 0.02$, $y = 0$	2.1115(11)	1.9644(10)	8.03	6.78
$x = 0$, $y = 0.01$	2.1108(13)	1.9666(11)	8.24	6.69
$x = 0$, $y = 0.02$	2.1104(15)	1.9668(12)	9.22	7.93
$x = 0.01$, $y = 0.01$	2.1102(11)	1.9664(12)	8.45	7.02

Evaluation of the structural and thermal stability of the Mg and Al-substituted $Li_{0.3}[Ni_{0.8}Co_{0.1}Mn_{0.1-x-y}Al_xMg_y]O_2$ material was carried out using the chemically delithiated samples ($Li_{0.3}[Ni_{0.8}Co_{0.1}Mn_{0.1-x-y}Al_xMg_y]O_2$: $x = 0.0$–0.02, $y = 0.0$–0.02). Fig. 6 shows the thermogravimetry (TG) and DTG curves (the

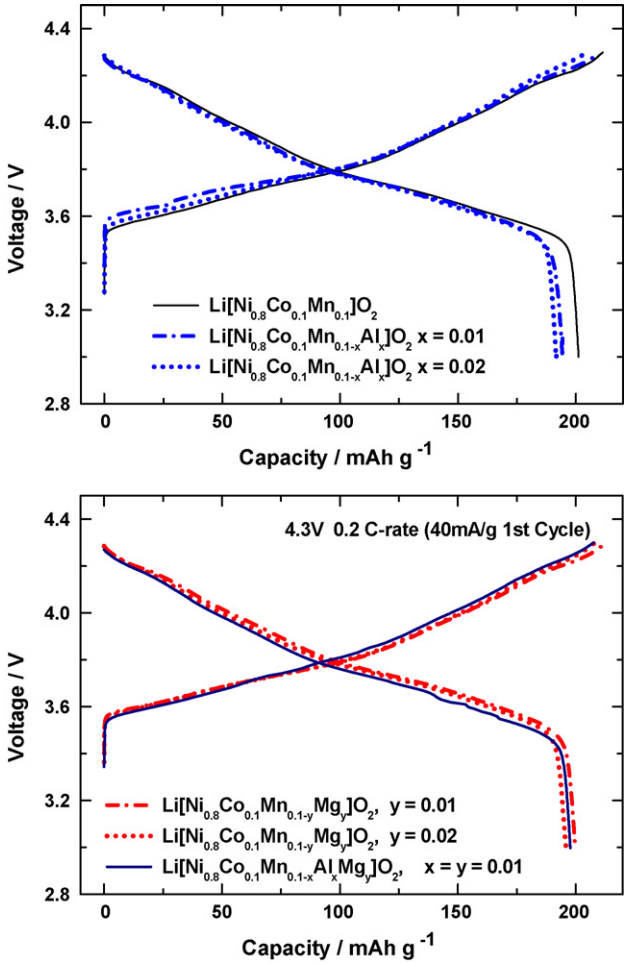

Fig. 4. Initial charge–discharge curves of $Li/Li[Ni_{0.8}Co_{0.1}Mn_{0.1-x-y}Al_xMg_y]O_2$ ($x = 0.0$–0.02, $y = 0.0$–0.02) cells at a constant current density of 40 mA g^{-1} (0.2 C-rate) in the range of 3.0 and 4.3 V.

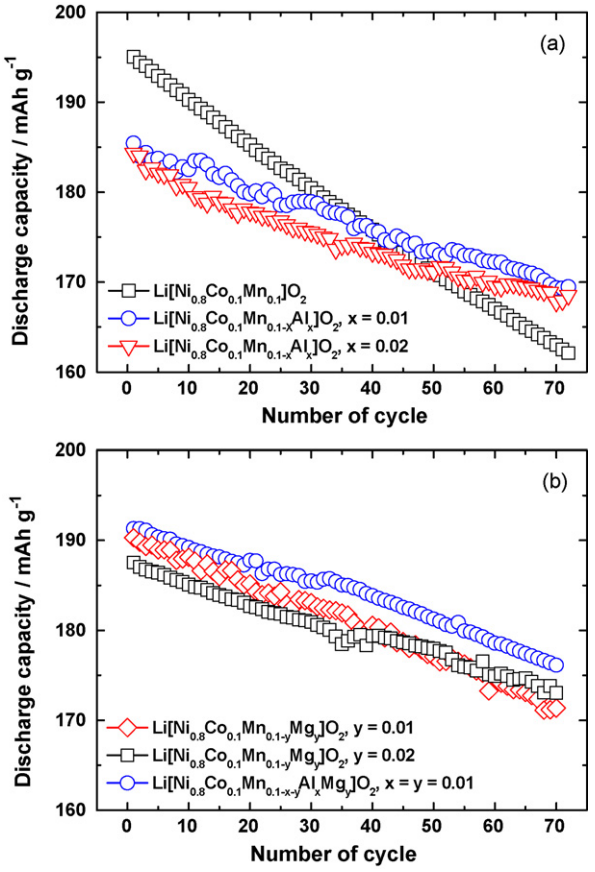

Fig. 5. Variation of discharge capacities of Li/Li[$Ni_{0.8}Co_{0.1}Mn_{0.1-x-y}Al_xMg_y$]$O_2$ cells: (a) $x = y = 0$, $x = 0.01$ and $y = 0$, $x = 0.02$ and $y = 0.0$, and (b) $x = y = 0.01$, $x = 0$ and $y = 0.01$, $x = 0$ and $y = 0.02$ as a function of cycle number cycled in the range of 3.0–4.3 V at a 0.5 C-rate (100 mA g^{-1}).

first derivative of the measured TG curves) of the chemically delithiated samples. The DTG curve in Fig. 6(b) shows the three steps of weight loss over the temperature range of 50–600 °C. The first step is mainly desorption of water occurring in temperature range of 90–150 °C featuring a small peak at 125 °C on the DTG curves for all samples. The second weight loss step occurred from 220 to 300 °C accompanied by weight losses of

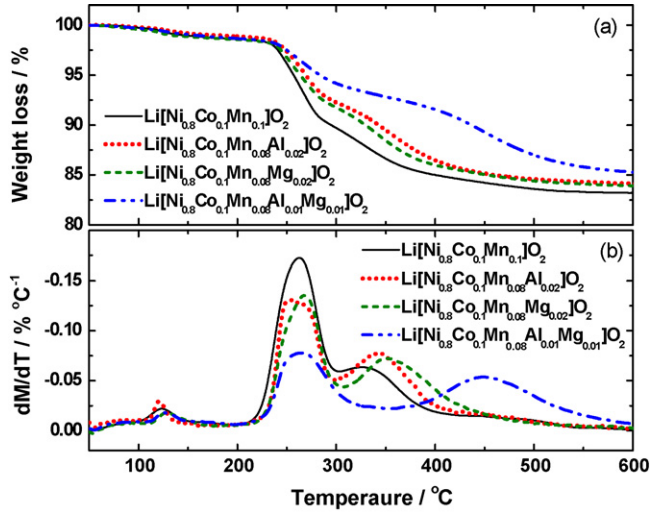

Fig. 6. (a) Thermogravimetry (TG) and (b) differential thermogravimetry (DTG) curves of chemically delithiated $Li_{0.3}[Ni_{0.8}Co_{0.1}Mn_{0.1-x-y}Al_xMg_y]O_2$ ($x, y = 0.0$–0.02).

9.2%, 5.9%, 7.8%, and 7.6% for $Li_{0.3}[Ni_{0.8}Co_{0.1}Mn_{0.1-x-y}Al_xMg_y]O_2$: $x = y = 0$, $x = 0.02$ and $y = 0$, $x = 0$ and $y = 0.02$, and $x = y = 0.01$, respectively. The weight loss rate of the second step was the most rapid and is attributed to the structural change of the delithiated positive electrode accompanying oxygen liberation and volatile combustion of the electrolyte with the liberated oxygen [40]. Among the samples, $Li_{0.3}[Ni_{0.8}Co_{0.1}Mn_{0.08}Al_{0.02}]O_2$ showed a relatively mild weight loss compared to the other samples, implying that the structural transformation was moderate. Also, both $Li_{0.3}[Ni_{0.8}Co_{0.1}Mn_{0.08}Mg_{0.02}]O_2$ and $Li_{0.3}[Ni_{0.8}Co_{0.1}Mn_{0.08}Al_{0.01}Mg_{0.01}]$ showed lower weight losses than $Li_{0.3}[Ni_{0.8}Co_{0.1}Mn_{0.1}]O_2$. After the second step, gradual weight loss in a step-wise manner (third step) was observed on the TG and DTG curves until 600 °C. The third step of the decomposition reaction, accompanied with weight loss, may be attributed to the reaction of the remaining electrolyte with the continuous decomposition of the positive electrode.

Thermal stability and safety of positive electrode at highly delithiated states are important concerns in determining the suitability of lithium batteries for practical applications. Fig. 7(a) shows the DSC profiles of the chemically delithiated Mg-substituted $Li_{0.3}[Ni_{0.8}Co_{0.1}Mn_{0.1-y}Mg_y]O_2$ materials ($y = 0.0$, 0.01, and 0.02) in the presence of electrolyte. All samples showed a major exothermal peak at around 214.7 °C, resulting from the decomposition reaction of the electrolyte with the oxygen released from the delithiated $Li_{0.3}[Ni_{0.8}Co_{0.1}Mn_{0.1-y}Mg_y]O_2$ [41], which was initiated by the structural transformation. The onset of the exothermic reaction did not significantly change with respect to the amount of the Mg doping. However, the magnitude of the major exothermic peak reduced as the amount of Mg doping increased. The heats generated from the exothermic reaction on the DSC traces in the temperature range of 110–350 °C were 1352 J g^{-1}, 968 J g^{-1}, and 1080 J g^{-1} for the $Li_{0.3}[Ni_{0.8}Co_{0.1}Mn_{0.1}]O_2$, $Li_{0.3}[Ni_{0.8}Co_{0.1}Mn_{0.09}Mg_{0.01}]O_2$, and $Li_{0.3}[Ni_{0.8}Co_{0.1}Mn_{0.08}Mg_{0.02}]O_2$, respectively. On the contrary, it is evident that the substitution of Al in the structure affects the DSC thermal behaviors in terms of the onset temperature as well as the exothermic heat generation. As shown in Fig. 7(b), the major exothermic peak detected at 214 °C for the $Li_{0.3}[Ni_{0.8}Co_{0.1}Mn_{0.1}]O_2$ sample shifted to 225 °C and 242.7 °C for $Li_{0.3}[Ni_{0.8}Co_{0.1}Mn_{0.09}Al_{0.01}]O_2$ and $Li_{0.3}[Ni_{0.8}Co_{0.1}Mn_{0.08}Al_{0.02}]O_2$, respectively. Also, the exothermic heat generation of the Al-

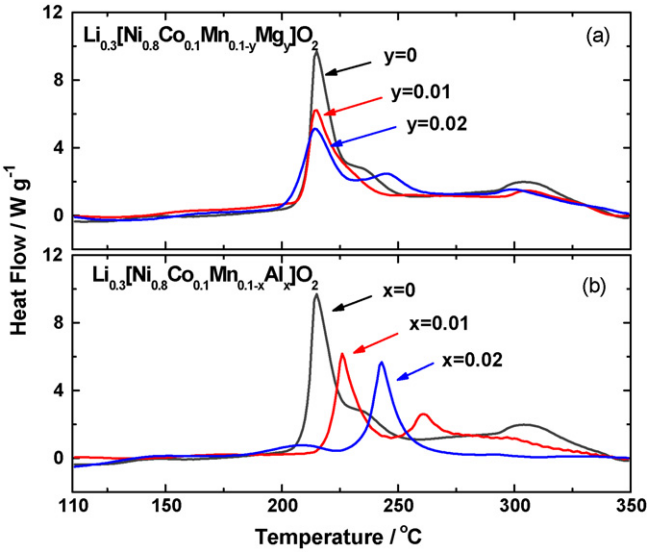

Fig. 7. Differential scanning calorimetry (DSC) traces of (a) Li[$Ni_{0.8}Co_{0.1}Mn_{0.8-y}Mg_y$]$O_2$ ($y = 0.0$, 0.01, and 0.02) and (b) Li[$Ni_{0.8}Co_{0.1}Mn_{0.C}Al_x$] ($x = 0.0$, 0.01, and 0.02) charged to 4.3 V at a scan rate of 5 °C min^{-1}.

substituted $Li_{0.3}[Ni_{0.8}Co_{0.1}Mn_{0.1-x}Al_x]O_2$ materials ($x = 0.01$ and $x = 0.02$) decreased as the content of Al increased with 1352 J g^{-1} for $x = 0$, 980 J g^{-1} for $x = 0.01$, and 956 J g^{-1} for $x = 0.02$. It was reported by Pouillerie et al. [42] that the preferential occupancy of magnesium ions in $Li[Ni_{0.86}Co_{0.09}Mg_{0.05}]O_2$ suppressed the expansion of the lattice along the *c*-axis during consecutive cycling at 60 °C. Consequently, improved structural integrity was achieved with Al substitution, as confirmed by structural refinement (Fig. 3) and cycling tests (Fig. 5). It has been known that such a structural stabilization led to improve the cycling behavior by suppressing phase transformation and to result in better thermally stability, as suggested by Ohzuku et al. [14,43]. Therefore, it can be concluded that the enhanced thermal stability of Al and Mg-substituted $Li_{1-x}[Ni_{0.8}Co_{0.1}Mn_{0.1-x-y}Al_xMg_y]O_2$ can be mainly attributed to the improved structural stability.

4. Conclusion

Al and/or Mg-substituted $Li[Ni_{0.8}Co_{0.1}Mn_{0.1-x-y}Al_xMg_y]O_2$ were prepared by a co-precipitation method and characterized by Rietveld refinement, thermogravimetry, DSC, and electrochemical measurements. Although the Al and/or Mg-substituted $Li[Ni_{0.8}Co_{0.1}Mn_{0.1-x-y}Al_xMg_y]O_2$ electrodes delivered somewhat lower initial discharge capacities, capacity retention, structural stability, and thermal stability were enhanced compared to the pristine $Li[Ni_{0.8}Co_{0.1}Mn_{0.1}]O_2$. The initial discharge capacity of the $Li[Ni_{0.8}Co_{0.1}Mn_{0.08}Al_{0.01}Mg_{0.01}]O_2$ was 191 mAh g^{-1}, showing only 7.5% capacity loss after 70 cycles. The reduced cation mixing and improved structural stability are due to the enhancement of cyclability and thermal stability caused by Al and Mg substitution.

Acknowledgments

This work was supported by Korea Science and Engineering Foundation (KOSEF) grant funded by the Korea government (MEST) (No. R11-2008-088-03002-0).

References

[1] M.G.S.R. Thomas, W.I.F. David, J.B. Goodenough, P. Groves, Mater. Res. Bull. 20 (1985) 1137.
[2] J.R. Dahn, U. von Sacken, C.A. Michal, Solid State Ionics 44 (87) (1990).
[3] J.R. Dahn, U. von Sacken, M.W. Juzkow, H. Al-Janaby, J. Electrochem. Soc. 138 (1991) 2207.
[4] C. Delmas, I. Saadoune, Solid State Ionics 53 (1992) 370.
[5] T. Ohzuku, A. Ueda, M. Nagayama, J. Electrochem. Soc. 140 (1993) 1862.
[6] C. Delmas, I. Saadoune, A. Rougier, J. Power Sources 44 (1993) 595.
[7] M. Menetrier, A. Rougier, C. Delmas, Solid State Commun. 90 (1994) 484.
[8] A. Ueda, T. Ohzuku, J. Electrochem. Soc. 141 (1994) 2010.
[9] A. Rougier, P. Gravereau, C. Delmas, J. Electrochem. Soc. 143 (1996) 1168.
[10] Y. Gao, M.V. Yakovleva, W.B. Ebner, Electrochem. Solid-State Lett. 1 (1998) 117.
[11] W. Ebner, D. Fouchard, L. Xie, Solid State Ionics 69 (1994) 238.
[12] J. Cho, G. Kim, G.H. Lim, J. Electrochem. Soc. 146 (1999) 3571.
[13] Q. Zhong, U. von Sacken., J. Power Sources 54 (1995) 221.
[14] T. Ohzuku, A. Ueda, M. Kouguchi, J. Electrochem. Soc. 142 (1995) 4033.
[15] G.X. Wang, S. Zhong, D.H. Bradhurst, S.X. Dou, H.K. Liu, Solid State Ionics 116 (1999) 271.
[16] C. Pouillerie, L. Croguennec, C. Delmas, Solid State Ionics 132 (2000) 15.
[17] C.-C. Chang, J.Y. Kim, P.N. Kumta, J. Electrochem. Soc. 147 (2000) 1722.
[18] J. Cho, Chem. Mater. 12 (2000) 3089.
[19] Y. Nishida, N. Kenji, T. Satoh, J. Power Sources 68 (1997) 561.
[20] Y. Sato, T. Koyano, M. Mukai, K. Kobayakawa, Denki Kagaku 66 (1998) 1215.
[21] H. Arai, S. Okada, Y. Sakurai, J. Yamaki, J. Electrochem. Soc. 144 (1997) 3117.
[22] S.H. Chang, S. Kang, S. Song, J. Yoon, J. Choy, Solid State Ionics 86–88 (1996) 171.
[23] Shim.F J., R. Kostecki, R. Richardson, X. Song, K.A. Striebel, J. Power Sources 112 (2002) 222.
[24] C.H. Chen, J. Liu, M.E. Stoll, G. Henriksen, D.R. Vissers, K. Amine, J. Power Sources 128 (2004) 278.
[25] S.-T. Myung, M.-H. Cho, H.-T. Hong, T.-H. Kang, C.-S. Kim, J. Power Sources 146 (2005) 222.
[26] Y. Itou, Y. Ukyo, J. Power Sources 146 (2005) 39.
[27] K. Amine, J. Liu, I. Belharouak, S.-H. Kang, I. Bloom, D. Vissers, G. Henriksen, J. Power Sources 149 (2005) 111.
[28] H. Kondo, Y. Takeuchi, T. Sasaki, S. Kawauchi, Y. Itou, O. Hiruta, C. Okuda, M. Yonemura, T. Kamiyama, Y. Ukyo, J. Power Sources 174 (2007) 1063.
[29] D.P. Abraham, S. Kawauchi, D.W. Dees, Electrochim. Acta 53 (2008) 2121.
[30] M.-H. Kim, H.-S. Shin, D. Shin, Y.-K. Sun, J. Power Sources 159 (2006) 1328.
[31] D. Caurant, N. Baffier, B. Garcia, J.P. Pereira-Ramos, Solid State Ionics 91 (1996) 45.
[32] M.-H. Lee, Y.-J. Kang, S.-T. Myung, Y.-K. Sun, Electrochim. Acta 50 (2004) 939.
[33] T. Roisnel, J. Rodriguez-Carjaval, Fullprof Manual, Institut Laue-Langevin, Grenoble, France, 2002.
[34] R.D. Shannon, Acta Crystallogr., Sect. A: Cryst. Phys., Diffr., Theor. Gen. Crystallogr. 32 (1976) 756.
[35] Joint Committee on Powder Diffraction Standard, File no. 19-713.
[36] S.-T. Myung, N. Kumagai, S. Komaba, H.-T. Chung, Solid State Ionics 139 (2001) 47.
[37] C. Pouillerie, L. Croguennec, Ph. Biensan, P. Willmann, C. Delmas, J. Electrochem. Soc. 147 (2000) 2061.
[38] J.A. Dean, Lange's Handbook of Chemistry, fourth ed., McGraw-Hill Inc., New York, 1992, p. 6.81.
[39] H. Tukamoto, A.R. West, J. Electrochem. Soc. 144 (1997) 3164.
[40] H.J. Bang, H. Joachin, H. Yang, K. Amine, J. Prakash, J. Electrochem. Soc. 153 (2006) A731.
[41] H. Arai, M. Tsuda, K. Saito, M. Hayashi, Y. Sakurai, J. Electrochem. Soc. 146 (2002) A401.
[42] C. Pouillerie, F. Perton, Ph. Biensan, J.P. Pérés, M. Broussely, C. Delmas, J. Power Sources 96 (2001) 293.
[43] T. Ohzuku, T. Yanagawa, M. Kouguchi, A. Ueda, J. Power Sources 68 (1997) 131.